Novel Monolithic All-Silicon Coherent Transceiver Sub-Assembly based on Ring Modulators

Youngkwan Jo, Matthieu Oberon, Anna Peczek, Yongjin Ji, Minkyu Kim, Hyun-Kyu Kim, Min-Hyeong Kim, Pascal M. Seiler, Stefan Lischke, Christian Mai, Lars Zimmermann and Woo-Young Choi

***Abstract*—We demonstrate a novel monolithic coherent transceiver sub-assembly based on ring modulators, realized with Si photonic BiCMOS technology which allows monolithic integration of Si photonic integrated circuits and high-performance BiCMOS electronics. The transmitter consists of a ring modulator assisted Mach-Zehnder interferometer (RaMZI) and modulator driver electronics. The complex electro-optic modulation characteristics of the Si ring modulators (RMs) used for the transmitter are carefully investigated. The receiver includes the photonic components such as the Ge photodiodes and multimode interferometer (MMI) as well as the receiver front-end electronics such as transimpedance amplifier (TIA), variable gain amplifier (VGA) and output buffers. The performance evaluation of the novel monolithic all-silicon coherent transceiver sub-assembly based on ring modulators is carried out with a 28-Gbaud quadrature-phase-shift keying (QPSK) modulation signal.**

***Index Terms*—Silicon photonics, Coherent optical transceiver, Si ring modulator, Electronic-photonic integrated circuit.**

This work was supported by Institute of Information & communications Technology Planning & Evaluation (IITP) grant funded by the Korea government (MSIT) (No.RS-2023-00222171, Development of Tbps/mm chiplet interface IP and silicon photonics technology for AI and vehicle SoC). (*Corresponding author: Woo-Young Choi*)

Youngkwan Jo, Yongjin Ji, Hyun-Kyu Kim and Woo-Young Choi are with the High-Speed Circuits and Systems Laboratory, Department of Electrical and Electronic Engineering, Yonsei University, 03722 Seoul, South Korea (e-mail: kwan0122@yonsei.ac.kr; yjji0314@yonsei.ac.kr; yonsei142026@yonsei.ac.kr; wchoi@yonsei.ac.kr).

Minkyu Kim was with the High-Speed Circuits and Systems Laboratory, Department of Electrical and Electronic Engineering, Yonsei University, 03722 Seoul, South Korea. He is now with IMEC, 3001 Leuven, Belgium (email: minkyu226@imec.be).

Min-Hyeong Kim was with the High-Speed Circuits and Systems Laboratory, Department of Electrical and Electronic Engineering, Yonsei University, 03722 Seoul, South Korea. He is now with Synopsys Korea Inc. 13494, Seongnam, Gyeonggi-do, South Korea (email: teramhkim@gmail.com).

Matthieu Oberon, Anna Peczek, Stefan Lischke and Christian Mai are with the IHP—Leibniz-Institut für Innovative Mikroelektronik, 15236 Frankfurt (O.), Germany (e-mail: oberon@ihp-microelectronics.com, peczek@ihp-microelectronics.com, cmai@ihpmicroelectronics.com; lischke@ihp-microelectronics.com).

Pascal M. Seiler and Lars Zimmermann are with the IHP—Leibniz-Institut für Innovative Mikroelektronik, 15236 Frankfurt (O.), Germany and also with Technische Universität Berlin, FG Silizium-Photonik, 10587 Berlin, Germany (e-mail: seiler@tu-berlin.de, lzimmermann@ihpmicroelectronics.com).

Color versions of one or more of the figures in this article are available online at http://ieeexplore.ieee.org

I. INTRODUCTION

Photonic integrated circuits based on planar silicon technology have seen tremendous development over the past 10 years [1]-[3]. The major driver behind these efforts are applications of transceivers in fiber optical communications. Here, silicon photonics has been used in direct detect as well as in coherent systems. At the transmitter side, Mach-Zehnder modulators have been studied most. However, silicon Mach-Zehnder modulators based on free-carrier dispersion exhibit some serious drawbacks because they tend to suffer from high power-consumption and a large footprint [4]. From early on, ring-resonator based modulators have therefore been investigated as a small footprint and more power-efficient alternative. In the context of coherent communication, ring-modulator (RM) assisted Mach-Zehnder structures were studied for QPSK [5], [6], revealing several limitations of RM driving, in particular with respect to temperature stability, linearity and optical power handling. Recent years have seen considerable improvement in RM-based high-speed modulation for C- and O-band, mainly implementing intensity modulation [7]-[9] but including phase modulation using RM assisted Mach-Zehnder structures [10]. Beside fiber optical communications systems targeting 100Gbaud or beyond, novel applications of silicon photonic such as in satellite laser communication links do not require extremely high-speed, but seek robust, small footprint, low mass, and power efficient transceiver implementations. In the frame of a recent European space project (H2020-SPACE-ORIONAS) [11], we studied the monolithic all-silicon implementation of a coherent receiver sub-assembly [12]. The work was motivated by the reduced assembly complexity of a monolithic solution in comparison with conventional photonic electronic co-packaging implementations such as using wire bond or flip-chip ball grid array (BGA) technology.

In this work, we investigate the performance of highly compact all-silicon coherent transceiver sub-assembly chipset. The chipset has been fabricated in IHP's photonic BiCMOS technology [13]. To achieve overall small footprint, we designed a ring-assisted Mach-Zehnder IQ modulator co-integrated monolithically with driving amplifiers. The transmitter is complemented by a silicon photonic coherent receiver monolithically co-integrated with transimpedance amplifiers. The all-silicon transmitter and receiver sub-assembly has been characterized in a back-to-back and in a fiber-optical link configuration. Previous studies of the performance of all silicon coherent transceiver sub-assemblies on an optical link (e.g. [14-18]) were chiefly implemented

using Mach-Zehnder IQ modulators and hybrid photonic-electronic co-integration technology such as wire bonding. However, the IQ modulators alone typically occupy several square millimeters. To our knowledge, this is the first-time evaluation of a monolithic all-silicon photonic-electronic coherent transceiver sub-assembly using a ring-assisted transmitter as well as a fully Si photonic receiver. For this, the RM's phase modulation characteristics are carefully investigated, and the performance optimization in terms of the structure is carried out. The performance of the coherent transmitter (CoTx) electronic-photonic integrated circuit (ePIC) is evaluated with the coherent receiver (CoRx) ePIC, both realized within the photonic BiCMOS technology. The CoTx ePIC characteristics have been reported in [19], but in this paper, more detailed explanations of the CoTx ePIC and its link performances with the CoRx ePIC are provided. This paper is organized as follows. In Section II, the phase modulation characteristics and the structure optimization of RM are given, and the BiCMOS RM driver electronics and structure of the CoTx ePIC are described. In Section III, the characteristics of the CoTx ePIC measured with the CoRx ePIC are provided. Finally, Section IV concludes the paper.

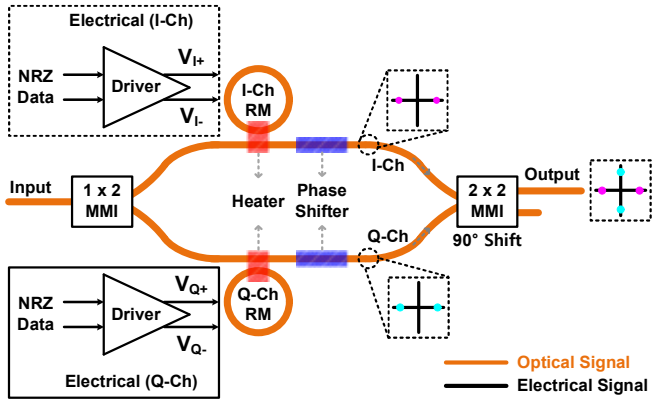

Fig 1. Schematic of a coherent transmitter ePIC with an IQ modulator based on a ring-assisted Mach-Zehnder interferometer and RM driver electronics.

II. Coherent Transmitter EPIC

Fig. 1 presents the schematic of a CoTx ePIC composed of a coherent IQ modulator and modulator driver electronics. The photonic components include a ring-assisted Mach-Zehnder interferometer (RaMZI) structure with two identical single-quadrature RMs in each arm, operating independently as the in-phase channel (I-Ch) or quadrature channel (Q-Ch). In a RaMZI, an optical signal split by a 1 x 2 multimode interferometer (MMI) is modulated by each RM and combined through a 2 x 2 MMI with a 90-degree phase difference, operating as the coherent IQ modulator. Integrated thermo-optic heaters and phase shifters solve the problems of resonance mismatch in RMs and arm length differences in MZI. The electronic circuits are a pair of RM driver electronics designed to amplify high-speed input non-return-to-zero (NRZ) signals to desired voltage for 180-degree phase shift (V_π) and differentially deliver them to RMs.

A. Phase Modulation Characteristics of RM

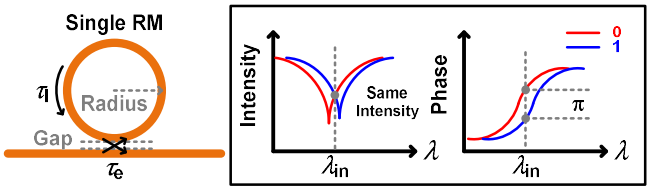

Fig 2. Schematic of phase-modulated single RM for either in-phase (I-Ch) or quadrature (Q-Ch) and its operation point for binary phase shift keying (BPSK) modulation.

Fig. 2 shows the structure of the single-quadrature RM, consisting of a ring waveguide and a bus waveguide. The modulation characteristics of the RM for the phase modulation can be characterized with the time-domain coupled-mode theory (CMT) approach as shown below [20]:

$$\frac{d}{dt}a(t) = (j\omega_{res} - \frac{1}{\tau})a(t) - j\sqrt{\frac{2}{\tau_e}}E_{in}(t), \quad (1)$$

$$E_{out}(t) = E_{in}(t) - j\sqrt{\frac{2}{\tau_e}}a(t), \quad (2)$$

where $a(t)$ represents the energy amplitude traveling in the ring waveguide, and τ is its decay time constant. τ is given as $(1/\tau_l + 1/\tau_e)^{-1}$ where τ_l and τ_e represent the decay time constants due to round-trip loss inside the ring waveguide and coupling loss around the directional coupler, respectively. ω_{res}, the resonant angular frequency, is given as $2\pi mc/n_{res}L$ where m is an integer, c is the speed of light in vacuum, n_{res} is the effective refractive index at resonance of the RM, and L is the circumference of the ring. $E_{in}(t)$ and $E_{out}(t)$ represent input and output signals of the RM, respectively.

The model parameter values depend on the structure of the RM. For example, the value of τ_l is dependent on the radius of the RM, and the value of τ_e is dependent on the coupling gap of the RM. For binary phase shift keying (BPSK) modulation, the RM should be over-coupling ($\tau_l > \tau_e$) so that π-phase shift can be achieved around the resonance wavelength with the same transmitted power when it is modulated with V_π as shown in Fig. 2.

The numerical values of τ_l, τ_e and n_{res} can be determined by fitting measured transmission characteristics to the steady-state transmission characteristics derived from (1) and (2) and show below [20],

$$T = \left|\frac{E_{out}}{E_{in}}\right|^2 = \left|\frac{j(\omega-\omega_{res}) + \frac{1}{\tau_l} - \frac{1}{\tau_e}}{j(\omega-\omega_{res}) + \frac{1}{\tau_l} + \frac{1}{\tau_e}}\right|^2. \quad (3)$$

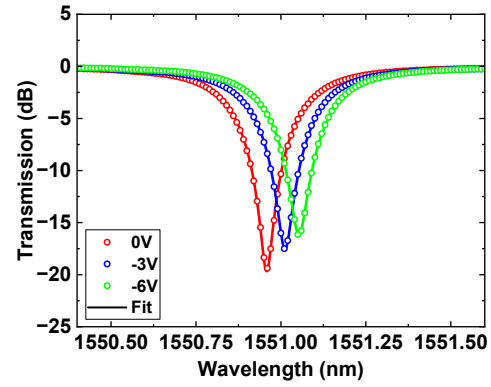

(a)

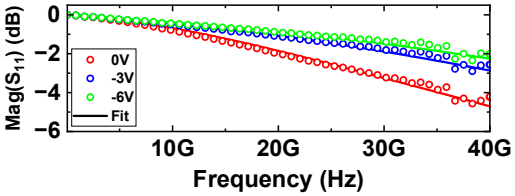

(b)

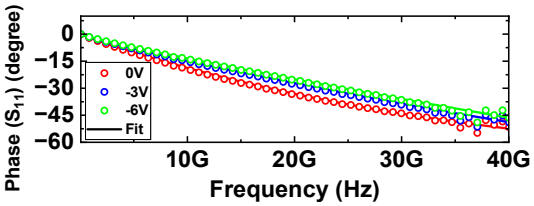

(c)

Fig 3. Measured and fitted (a) optical transmission spectra, (b) magnitude and (c) phase of electrical reflection coefficient (S_{11}) of Si RM at different bias voltages.

Fig. 3(a) shows the optical transmission spectra measured at different bias voltages for a sample RM. This RM has a 16-μm radius and a 220-nm coupling gap between ring and bus waveguides. 500 nm wide and 220 nm thick rib waveguides are used with a 100 nm slab thickness. The PN junction inside the RM has the nominal doping concentrations of 7×10^{17} cm^{-3} for the p-region and 3×10^{18} cm^{-3} for the n-region.

Furthermore, the electrical characteristics of RMs can be described with series resistance (R_s) and junction capacitance (C_j) of the RM PN junction [20]. Numerical values for these parameters can be determined from the measurement of the electrical reflection coefficient (S_{11}) as in shown Fig. 3(b) and (c). The extracted values of the optical parameters, τ_i, τ_e and n_{res}, as well as the electrical parameters, R_s and C_j, are listed in Table I.

The free-spectral range (FSR) of the sample RM is 6.24 nm, and the electro-optic resonance tuning efficiency ($\Delta\lambda_{res}$/V) is 15.1 pm/V from 0 V to 6 V. The dynamic insertion loss (IL) and V_π are 10.0 dB and 5.7 V, respectively, at λ_{in} of 1551.01 nm.

Fig. 4 shows the measured and simulated normalized electro-optic (E/O) responses of the same RM. For simulation, the time-domain response, $E_{out}(t)$, is first numerically calculated by solving (1) and (2) with the given parameter values. Then, $E_{out}(t)$ is Fourier-transformed to determine the complex E/O response. For complex E/O response measurement, RF signals having V_π peak-to-peak voltage are supplied to the RM with the reverse bias voltage at half V_π. Then, the modulated RM output signal is fed to the commercial coherent receiver with the heterodyne reception capability. The output signals of the coherent receiver, I+ and

TABLE I
EXTRACTED MODEL PARAMETERS OF SI RM

Bias (V)	n_{res}	τ_i (ps)	τ_e (ps)	R_s (Ω)	C_j (fF)
0	2.607275	21.4635	17.5920	105.7	34.96
-1	2.607314	22.0344	17.5922		30.58
-2	2.607340	22.4142	17.5924		28.00
-3	2.607366	22.6938	17.5926		26.21
-4	2.607389	23.0973	17.5927		24.84
-5	2.607412	23.3947	17.5929		23.74
-6	2.607435	23.7619	17.5930		22.81

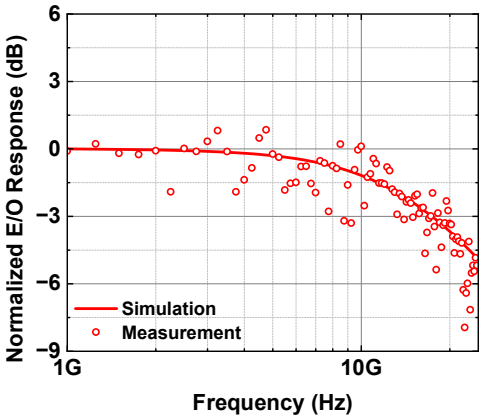

(a)

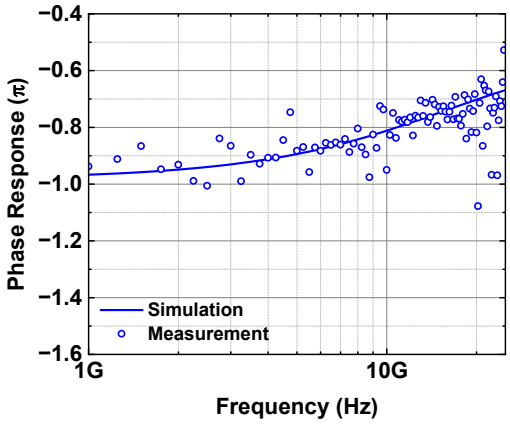

(b)

Fig 4. Measured and simulated (a) normalized magnitude response and (b) phase response of Si RM with the reverse bias voltage at half V_π. The model parameters from Table I are used to generate the simulated data.

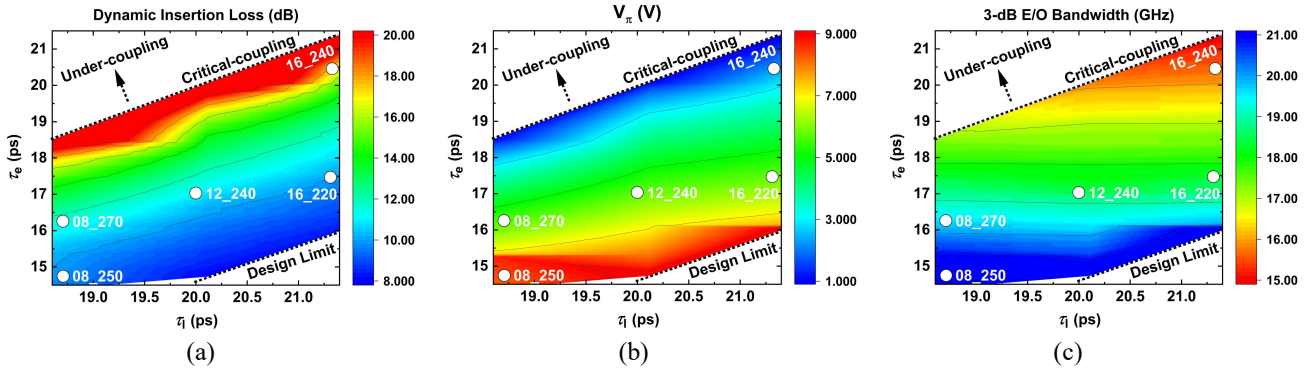

Fig 5. Performance investigation of single RMs in terms of τ_l and τ_e at 0 V. (a) Dynamic insertion loss in dB, (b) V_π in V and (c) 3-dB E/O bandwidth in GHz. The circles indicate the measured result of the fabricated RMs.

TABLE II
MEASURED AND SIMULATED V_π, INSERTION LOSS AND 3-DB E/O BANDWIDTH FOR 5 DIFFERENT RMS.

Radius [μm]		8	8	12	***16***	16
Coupling Gap [nm]		250	270	240	***220***	240
Device		08_250	08_270	12_240	***16_220***	16_240
V_π (V)	Measured	7.7	5.4	6	***5.7***	2.8
	Simulated	8.09	5.53	5.93	***5.65***	2.25
Dynamic insertion loss (dB)	Measured	10.63	11.92	10.63	***10.0***	15.66
	Simulated	9.7	11.7	10.6	***10.1***	16.6
3-dB E/O bandwidth (GHz)	Measured	21.5	19.5	19.25	***18.5***	14.75
	Simulated	22	19.6	18.8	***18.2***	15.6

Q+, are acquired using a real-time oscilloscope for off-line digital signal processing (DSP), with which compensation for the carrier frequency offset and bandpass filtering for eliminating the out-of-band noise are carried out [21]. Then, the resulting signals are Fourier-transformed for frequency-domain analysis [20]. The responses of the RF amplifier, cables, probes as well as the commercial coherent receiver are all de-embedded. The measured and the simulated results shown in Fig. 4 have some discrepancies due to the fair amount of error signals in the measurement results that are believed to be due to insufficient de-embedding of the coherent receiver, but there is an agreement for an overall trend, from which the 3-dB bandwidth of the E/O response can be estimated to be 18.5 GHz.

B. Structure Optimization of RM

The modulation characteristics of RMs mainly depend on the structure parameters such as the radius and the coupling gap, resulting in the different values of model parameters. In addition to the sample RM, RMs with different model parameters are also investigated so that their influence on the performance can be analyzed. For identification, these RMs are labeled with their "radius" and "coupling gap". For example, "16_220" represents a RM with 16-μm radius and 220-nm coupling gap, which is the RM sample discussed in Section II-A.

The simulated dynamic IL, V_π and 3-dB E/O bandwidth are shown in the Fig. 5(a), (b) and (c), respectively. The circles in Fig. 5 show the measured results for 5 fabricated RMs. In the figure, the under-coupled ($\tau_l < \tau_e$) RMs are excluded because π-phase shift cannot be achieved. In contrast, because the critically coupled ($\tau_l = \tau_e$) RMs have more abrupt 2π-phase shift around the resonance, the required π-phase shift is achieved with a lower V_π, but the IL becomes very large due to the sharper notch characteristics, as can be seen in Fig. 5(a) and (b). Higher 3-dB E/O modulation bandwidth can be achieved if lower values of τ_l and τ_e are used as can be seen in Fig. 5(c) where the bottom-left region with lower values of τ_l and τ_e shows higher 3-dB E/O bandwidth. However, such RMs require very large driving voltages exceeding the maximum output voltage swing of our BiCMOS driver circuits. Furthermore, a low τ_e value requires a RM with a small coupling gap which is limited by the minimum space requirement for two rib waveguides in the design rule of our Si photonic process. With process-level efforts such as realizing the vertical PN junction diode structure and further optimized carrier concentrations, Si RMs with higher E/O modulation efficiency (Δn_{res}/V) can be realized, which can alleviate the burden of high driving voltage required for RMs

with higher bandwidth. As can be seen in Fig. 5, "08_250" requires a high V_π larger than the maximum output peak-to-peak voltage of the BiCMOS driver electronics. In addition, "16_240" has lower E/O bandwidth and higher IL compared to others. For these reasons, "16_220" RM is selected as the structure to be used in our CoTx ePIC. Table II shows the details of measured and simulated performance parameters for various RMs.

C. RM Driver Electronics and Fabricated CoTx ePIC

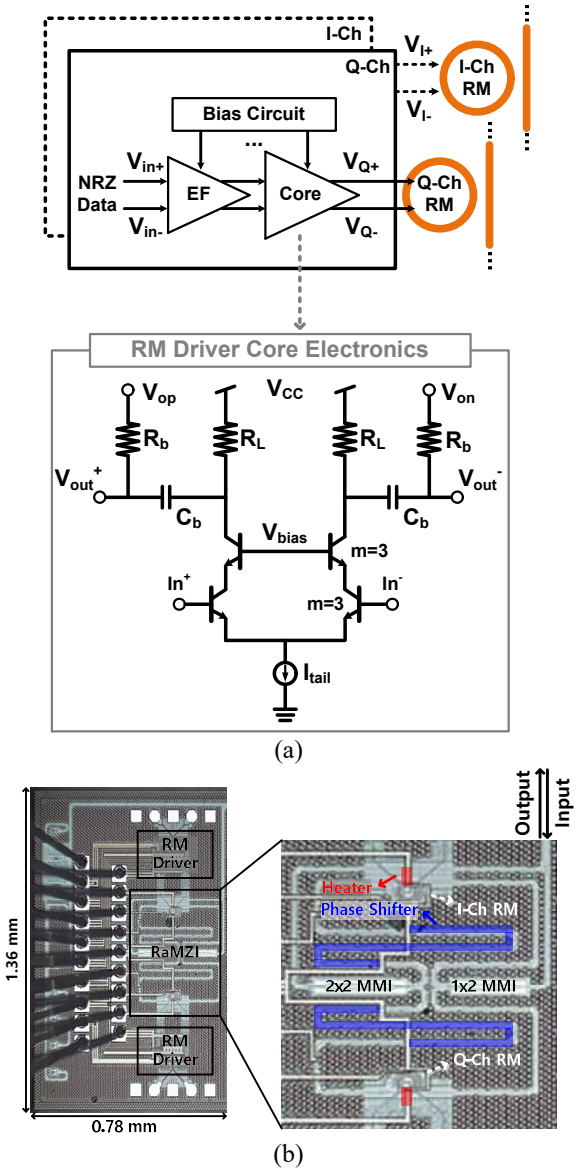

Fig 6. (a) Schematic of BiCMOS RM driver electronics for RaMZI in the Si CoTx ePIC and (b) chip micro photo of the fabricated CoTx ePIC.

Fig. 6(a) shows the structure of BiCMOS RM driver electronics for RaMZI in Si CoTx ePIC, which is designed for independently supplying the electrical signal with the required voltage (V_π) for the 180-degree phase modulation to each RM at the target data rate. In the drivers, emitter followers are used to buffer the electrical signal to the next stage, and the driver core based on the fully differential cascode structure can deliver up to 6 $V_{peak\text{-}to\text{-}peak,diff}$ to the RM [19]. The bias voltages for the driver are provided by bias circuits composed of an operational transconductance amplifier and a replica circuit of the driver core. The biases for the RMs are externally supplied from the output stage of the driver with a capacitive coupling.

Fig. 6(b) shows the chip micro photo of the fabricated CoTx ePIC, in which two interferometric paths as well as RMs are shown with different colors for clarity. In a RaMZI, the optical input signal is divided into two arms with a 1 × 2 MMI coupler, and the divided signals pass through identical RMs in two arms, one for I-Ch and the other for Q-Ch. The RMs are optimized to generate the 28-Gbaud BPSK signal as described in Section II-B. Due to process variation, two RMs typically have slightly different resonance wavelengths. This difference can be compensated by aligning the resonance wavelength of two RMs using the Si on-chip heaters integrated in the directional coupler regions of two RMs. In addition, there is a difference in the arm length of the MZI also due to process variation. This difference is compensated by metal heaters integrated on the top of two MZI arms. To cover half of the FSR, 45.7 mW of power is required for the heater, and to cover 2π phase mismatch of the MZI, 57.9 mW of power is required for the phase shifter. The two BPSK signals generated by two RMs are combined with a 2 × 2 MMI that provide 90° phase shift, resulting in QPSK signals.

III. Measurement of a Transmitter EPIC with a Receiver EPIC

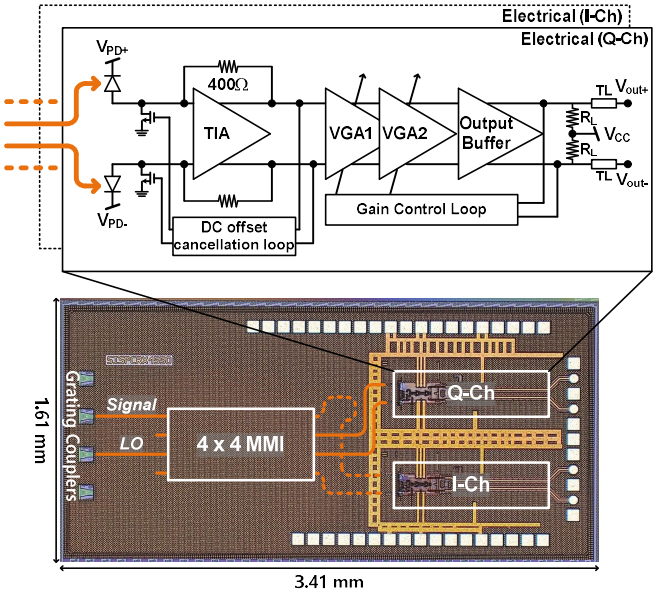

Fig 7. Chip micro photo and schematic of Si coherent receiver (CoRx) ePIC.

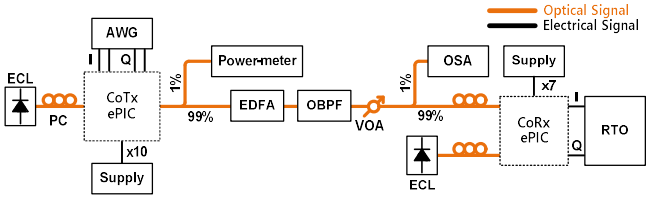

Fig 8. Measurement setup for bit-error rate (BER) versus received optical power (ROP). (ECL: external-cavity laser, EDFA: erbium-doped fiber amplifier, PC: polarization controller, AWG: arbitrary waveform generator, VOA: variable optical attenuator, OSA: optical spectrum analyzer, OBPF: optical bandpass filter, RTO: real-time oscilloscope.)

Fig. 7 shows the chip microphotograph and device schematic of the fabricated Si CoRx ePIC. The typical 3 dB opto-electrical bandwidth of the CoRx ePIC with similar design have been shown to be around 30 GHz [23], [24]. The grating couplers (GCs) are used as optical I/O. The 90° hybrid is realized with a 4 × 4 MMI, and the design of the MMI is based on the one found in [25] with a 189-μm length and 10-μm width. The outputs of MMI are terminated by single-ended Ge photodiodes which are in turn connected to the electrical circuit. The circuit design is based on those found in [26], [27]. The electrical output stage per channel consists of a trans-impedance amplifier (TIA), two variable gain amplifiers (VGA), a 50 Ω output buffer with differential output, gain control loop and a DC offset cancellation loop. The electrical circuit features a fully differential input transimpedance stage which allows the mismatch between the single-ended photodiodes to be compensated by the DC offset cancellation loop. Further information can be found in [26], [27].

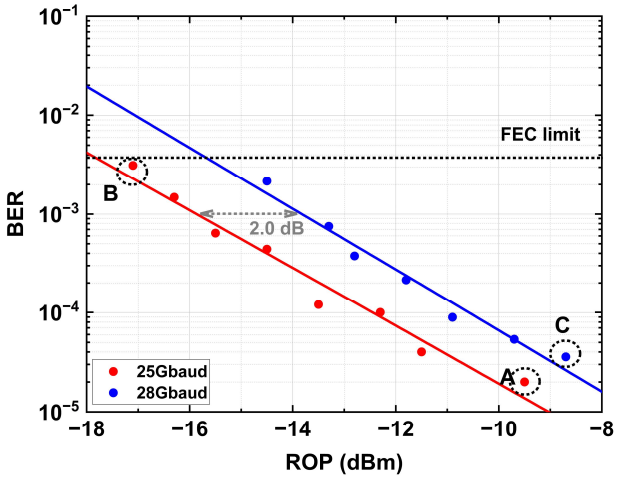

Fig 9. Measured BER vs ROP with CoTx ePIC and CoRx ePIC. In the figure, Point A, B and C denote the measured cases with A: 25Gbaud, ROP = -9.5dBm, B: 25Gbaud, ROP = -17.1dBm and C: 28Gbaud, ROP = -8.7dBm.

Fig. 8 shows the measurement setup used for the bit-error rate (BER) in terms of received optical power (ROP). Unlike fiber-based coherent transceivers, the ROP constitutes an important performance metric in free-space optical (FSO) communication, as it can be used in conjunction with the statistics of turbulence-induced-fades in order to determine the mean BER of such a link [28], [29]. The electrical 28-Gbaud QPSK signals with root-raised cosine filtering whose roll-off factor is 1.0 are generated by an arbitrary waveform generator (AWG, Keysight M8199A, 256 Gs/s) and introduced to the

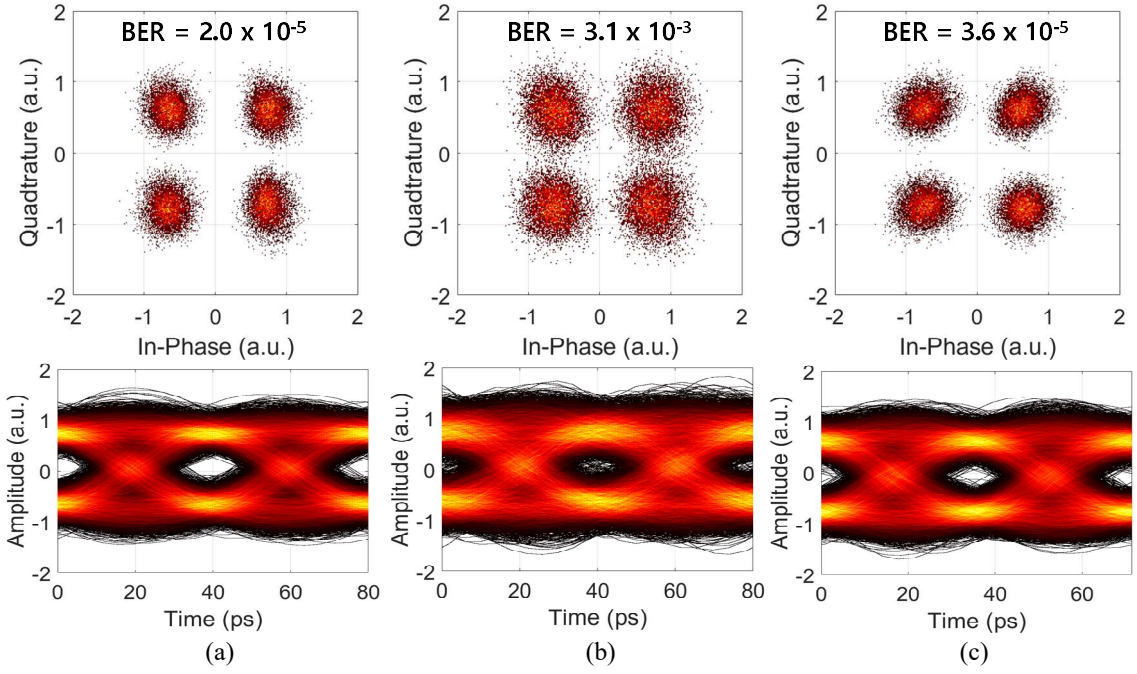

Fig 10. Recovered constellations and I-Ch eye diagrams with CoTx ePIC and CoRx ePIC for (a) 25Gbaud, ROP = -9.5dBm (Point A in Fig. 9), (b) 25Gbaud, ROP = -17.1dBm (Point B in Fig. 9) and (c) 28Gbaud, ROP = -8.7dBm (Point C in Fig. 9). The eye diagrams have been resampled, and the data are color-coded to their bin count.

TABLE III
PERFORMANCE COMPARISON OF SI COHERENT TRANSCEIVER SUB-ASSEMBLY.

		[14-17]	[18]	This work
Process	Tx EIC	GF 9HP 90-nm BiCMOS	130-nm SiGe BiCMOS	IHP 0.25-μm Si Photonic BiCMOS
	Rx EIC	GF 8XP 130-nm BiCMOS		
	PIC	Intel Si Photonics	N/A	
Optical Band		O-band	C-band	C-band
Link Configuration		Tx + Rx sub-assemblies with analog equalization	Flip-chipped transceiver with off-line DSP	Tx + Rx sub-assemblies with off-line DSP
Modulation Format		DP-QPSK	SP- and DP-QPSK SP- and DP-16QAM DP-64QAM	SP-QPSK
Demonstrated Baud-rate		56 Gbaud	69 Gbaud for DP-16QAM	28 Gbaud
Driver Integration		Hybrid	Hybrid	Monolithic
Device Structure		MZM	MZM	Ring-assisted MZI
Chip Size	Tx	41.4 mm^2 (*)	~20 mm^2 (**)	1.06 mm^2
	Rx	~21 mm^2 (**)	~10 mm^2 (**)	5.49 mm^2
Power Consumption	Tx	1,200 mW (DP)	4,000 mW (DP)	986.3 mW
	Rx	900 mW (DP)	1,100 mW (DP)	518 mW
Energy efficiency at 28 Gbaud (Min. demonstrated)	Tx	10.7 pJ/bit (5.4 pJ/bit)	35 pJ/bit (7.2 pJ/bit)	17.6 pJ/bit
	Rx	8.0 pJ/bit (4.0 pJ/bit)	9.8 pJ/bit (2.0 pJ/bit)	9.3 pJ/bit (2.0 pJ/bit [23])

(*) Tx PIC includes semiconductor optical amplifier (SOA) integration.
(**) Estimation calculated using the micrograph and the reported size of the EIC.

CoTx ePIC through a pair of RF probes so that the required V_π is delivered to the RMs. The CoTx ePIC chip is mounted on a FR4 printed circuit board, which provides the necessary biases for optical devices and the BiCMOS driver. The biases for the CoRx ePIC are directly supplied from the DC probes. The bias voltages for the heater and the phase shifter are determined so that the resonances of two RMs coincide at the same wavelength, and the quadrature phase difference after the 2 × 2 MMI is achieved with the 3-dB drop from the maximum output optical power. The operation wavelength, λ_{in}, for BER evaluation for the CoTx ePIC is 1548.38 nm which is different from λ_{in} of 1551.01 nm in Fig. 3(a) due to process variations. The performance variation of RMs due to process variations is assumed to be negligible within several nanometers. As described in Section II-C, the RaMZI can be aligned for QPSK operation with the heater and phase shifter. The CoTx ePIC consumes 986.3 mW of power for 28-Gbaud QPSK operation which includes power consumption of the heater (6.4 mW) and the phase shifter (11.4mW), and the CoRx ePIC consumes 518 mW for 28-Gbaud operation.

The optical inputs for the CoTx and local oscillator (LO) of the CoRx are supplied from the external cavity laser (ECL). Their optical powers are +3 dBm for the CoTx and +8 dBm for the LO of the CoRx. The insertion loss of CoTx is measured as 27.8 dB including 12.5 dB of coupling loss for the pair of GCs of the CoTx. The output of CoTx is delivered to the CoRx, after amplified by the erbium-doped fiber amplifier (EDFA) and filtered by the optical bandpass filter (OBPF) with 0.8nm bandwidth. The variable optical attenuator (VOA) is used to control the ROP for the CoRx. The coupling losses for the CoRx are 3.8 dB for each GC, and the fiber loss between the VOA output and the CoRx input and fiber array loss are de-embedded in the latter description in ROP. The polarizations for each GC are optimized to obtain the maximum output power for single polarization (SP) operation, and the data capacity can be further increased with 2-D grating couplers [30] for dual-polarization (DP) which has been demonstrated in the receiver ePIC with the same technology [24]. The output signals (I+ and Q+) of CoRx are acquired by RF probes and a real-time oscilloscope (RTO, Tektronix DPO77002SX). For off-line DSP, a communication analyzer tool (Tektronix OM1106) is used. The DSP includes clock recovery, root-raised cosine filtering, carrier phase estimation [31] and least-mean square adaptive equalization using the constant modulus algorithm [32].

Fig. 9 presents the measured bit-error rate (BER) of the CoTx ePIC and CoRx ePIC link for 25-Gbaud and 28-Gbaud QPSK operations in terms of the ROPs. The recovered constellations and resampled I-Ch eye diagrams for the measured points in Fig. 9 are shown in Fig. 10. The BER performance achieved below the forward-error correction (FEC) limit demonstrates the successful operations for both 25 Gbaud and 28 Gbaud. The ROP penalty between 25-Gbaud and 28-Gbaud operations is found to be 2.0 dB. This penalty is attributed mostly to the bandwidth of the CoTx, which is primarily limited by the E/O response of RM.

Table III compares the performance of Si coherent transceiver sub-assembly ePIC with recently reported results. The coherent transceiver sub-assembly links reported in [14-18] have been demonstrated for higher data rates with higher baud rates, higher-order modulation and DP configuration. For instance, the coherent link in [14-17] utilized analog

equalization technique based on Costas-loop optical phase-locked loop for O-band 56-Gbaud DP-QPSK operation. In addition, the coherent link in [18] have been realized with flip-chip integration for C-band 64-Gbaud DP-QPSK, 69-Gbaud DP-16QAM and 34-Gbaud DP-64QAM operation.

However, the sizes of these transmitters and receivers are significantly larger than the coherent transceiver sub-assembly ePICs presented in this work. The transmitter reported in [14-17] has PIC of 37.5 mm² and EIC of 3.9 mm², and the transmitter in [18] has PIC of ~18.4 mm² and EIC of 1.6 mm² where PIC size has been estimated from EIC size in [18]. In contrast, the CoTx ePIC in this paper has the photonic part of 0.16 mm² and the electronic part of 0.9 mm², resulting in the total chip area of 1.06 mm², which is much smaller than any coherent transmitters previously reported in [14-18]. This is because it is based on RaMZI for IQ modulator with co-integrated BiCMOS driver electronics, whereas other transmitters are based on hybrid integration of MZM and driver electronics. In the RaMZI structure, the RM reduces the phase shifter length thanks to the inherent phase response of RM, which corresponds to several millimeters in length in the MZM. In addition, the monolithic integration eliminates unnecessary device footprint increase caused by external electrical connection between PIC and EIC, minimizing the device footprint of transmitters. The transmitter sizes in [14-17] and [18] can respectively be halved to 20.7 mm² and ~10 mm² for a fair comparison because the CoTx ePIC in this work is designed for SP operation, while the transmitters in [14-18] have been designed for DP operation. Despite halving the sizes of the transmitters, it is evident that the CoTx ePIC has a smaller device footprint than the transmitters in [14-18]. Similarly, the receiver sizes in [14-17] and [18] are larger than the CoRx ePIC utilized in this work. In addition, the device footprint can be further reduced if the CoTx ePIC and CoRx ePIC are integrated into a single die because they are realized within the same photonic BiCMOS process, unlike the works in [14-17].

Power consumptions and energy efficiencies for 28-Gbaud operation and demonstrated minimum values are also compared in the table. The transmitter in this paper has lower energy efficiency compared to the transmitter reported in [14-17] is because the driving voltage for the modulator in [14-17] is 2 $V_{peak\text{-}to\text{-}peak}$, which is much smaller than the driving voltage for our modulator, 5.7 $V_{peak\text{-}to\text{-}peak}$. This is due to the low values of E/O modulation efficiency (Δn_{res}/V) as described in Section II-B, and process-level optimizations for higher value of Δn_{res}/V can alleviate the required high driving voltage for higher E/O modulation bandwidth, improving energy efficiency of the transmitter. The CoRx ePIC has the highest energy efficiency compared to the receiver in [14-18], considering the higher data rate of the CoRx ePIC with higher baud rate and DP operation demonstrated in [24].

IV. Conclusion

The novel monolithic all-silicon coherent transceiver sub-assembly based on ring modulators is demonstrated for 28-Gbaud QPSK operation realized within 0.25-μm Si photonic BiCMOS technology. The CoTx ePIC consists of the RaMZI and the BiCMOS driver electronics. The complex E/O response of the Si RM, a key building block of the CoTx ePIC, is characterized, and their performances dependence on the structure is investigated for performance optimization. The CoRx ePIC is composed of the optical components such as 4 x 4 MMI, Ge photodiodes as well as the BiCMOS receiver electronics. The data throughput can be further increased by the expansion of the suggested transceiver sub-assembly to the dual-polarization configuration for 100-Gbps data capacity requirement, which is currently under discussion for satellite laser communication links. The realized all-silicon coherent transceiver sub-assembly is measured in a back-to-back and fiber-optical link configuration, which confirms the potential of coherent satellite laser communications link by the photonic BiCMOS technology with the reduced device footprint.

Acknowledgment

The authors would like to thank IC Design Education Center (IDEC) for EDA tool support.

References

[1] S. Y. Siew et al., “Review of Silicon Photonics Technology and Platform Development,” Journal of Lightwave Technology, vol. 39, no. 13. Institute of Electrical and Electronics Engineers Inc., pp. 4374–4389, Jul. 01, 2021. doi: 10.1109/JLT.2021.3066203.

[2] G. T. Reed, G. Mashanovich, F. Y. Gardes, and D. J. Thomson, “Silicon optical modulators,” Nature Photonics, vol. 4, no. 8. pp. 518–526, Aug. 2010. doi: 10.1038/nphoton.2010.179.D

[3] S. Lischke et al., “Ultra-fast germanium photodiode with 3-dB bandwidth of 265 GHz,” Nat Photonics, vol. 15, no. 12, pp. 925–931, Dec. 2021, doi: 10.1038/s41566-021-00893-w.D

[4] L. Zimmermann et al., "Monolithically integrated 10Gbit/sec Silicon modulator with driver in 0.25µm SiGe:C BiCMOS," 39th European Conference and Exhibition on Optical Communication (ECOC 2013), London, 2013, pp. 1-3, doi: 10.1049/cp.2013.1441.

[5] P. Dong, C. Xie, L. Chen, N. K. Fontaine, and Y. Chen, “Experimental demonstration of microring quadrature phase-shift keying modulators,” Opt Lett, vol. 37, no. 7, p. 1178, 2012, doi: 10.1364/ol.37.001178.

[6] P. Dong, C. Xie, L. L. Buhl and Y. -K. Chen, "Silicon microring modulators for advanced modulation formats," 2013 Optical Fiber Communication Conference and Exposition and the National Fiber Optic Engineers Conference (OFC/NFOEC), Anaheim, CA, USA, 2013, pp. 1-3, doi: 10.1364/OFC.2013.OW4J.2.

[7] Y. Zhang et al., “200 Gbit/s Optical PAM4 Modulation Based on Silicon Microring Modulator,” in 2020 European Conference on Optical Communications, ECOC 2020, Institute of Electrical and Electronics Engineers Inc., Dec. 2020. doi: 10.1109/ECOC48923.2020.9333187.

[8] X. Wu et al., “A Single-Chip High-Speed Silicon Photonic Transmitter with Integrated Laser and Micro-Ring Modulator,” in IEEE International Conference on Group IV Photonics GFP, IEEE Computer Society, 2023. doi: 10.1109/SiPhotonics55903.2023.10141969.

[9] D. W. U. Chan, X. Wu, Z. Zhang, C. Lu, A. P. T. Lau, and H. K. Tsang, “C-band 67 GHz silicon photonic microring modulator for dispersion-uncompensated 100 Gbaud PAM-4,” Opt Lett, vol. 47, no. 11, p. 2935, Jun. 2022, doi: 10.1364/ol.460602.

[10] A. Geravand, Z. Zheng, S. Levasseur, L. A. Rusch, and W. Shi, “Ultra-Compact Silicon Modulator for 124 GBaud Coherent Optical Links,” in IEEE International Conference on Group IV Photonics GFP, IEEE Computer Society, 2023. doi: 10.1109/SiPhotonics55903.2023.10141908.

[11] L. Stampoulidis et al., “The H2020-SPACE-ORIONAS project: ‘Lasercom-on-chip’ for high-speed satellite constellation interconnectivity,” SPIE-Intl Soc Optical Eng, Jun. 2021, p. 57. doi: 10.1117/12.2599248.

[12] A. Osman et al., "First 100 Gb/s monolithically integrated electronic-photonic coherent receiver with direct edge coupling to standard single

mode fiber array," 2023 Optical Fiber Communications Conference and Exhibition (OFC), San Diego, CA, USA, 2023, pp. 1-3, doi: 10.1364/OFC.2023.M3I.3.

[13] S. Lischke, D. Knoll, C. Mai, and L. Zimmermann, "Advanced photonic BiCMOS technology with high-performance Ge photo detectors," SPIE-Intl Soc Optical Eng, Sep. 2019, p. 20. doi: 10.1117/12.2530143.

[14] A. Maharry et al., "First Demonstration of an O-Band Coherent Link for Intra-Data Center Applications," in Journal of Lightwave Technology, vol. 41, no. 21, pp. 6643-6650, 1 Nov.1, 2023, doi: 10.1109/JLT.2023.3290487.

[15] J. Liu et al., "First O-band silicon coherent transmitter with integrated hybrid tunable laser and SOAs," SPIE-Intl Soc Optical Eng, Mar. 2023, p. 49. doi: 10.1117/12.2668010.

[16] H. Andrade, A. Maharry, L. Valenzuela, N. Hosseinzadeh, C. Schow, and J. Buckwalter, "An 8.2-pJ/bit, 56 Gb/s Traveling-wave Modulator Driver with Large Reverse Terminations", in 2021 IEEE BiCMOS and Compound Semiconductor Integrated Circuits and Technology Symposium (BCICTS), Dec. 2021, pp. 1–4. DOI: 10.1109/BCICTS50416.2021.9682462.

[17] L. A. Valenzuela, Y. Xia, A. Maharry, H. Andrade, C. L. Schow, and J. F. Buckwalter, "A 50-GBaud QPSK Optical Receiver with a Phase/Frequency Detector for Energy- Efficient Intra-data Center Interconnects", IEEE Open Journal of the Solid-State Circuits Society, pp. 1–1, 2022, Conference Name: IEEE Open Journal of the Solid-State Circuits Society, ISSN: 2644-1349. DOI: 10.1109/OJSSCS.2022.3150291.

[18] A. H. Ahmed, A. E. Moznine, D. Lim, Y. Ma, A. Rylyakov and S. Shekhar, "A Dual-Polarization Silicon-Photonic Coherent Transmitter Supporting 552 Gb/s/wavelength," in IEEE Journal of Solid-State Circuits, vol. 55, no. 9, pp. 2597-2608, Sept. 2020, doi: 10.1109/JSSC.2020.2988399.

[19] Y. Jo et al., "A Si Photonic BiCMOS Coherent QPSK Transmitter Based on Parallel-Dual Ring Modulators," in IEEE International Conference on Group IV Photonics GFP, IEEE Computer Society, 2023. doi: 10.1109/SiPhotonics55903.2023.10141915.

[20] Y. Jo, C. Mai, S. Lischke, Z. Lars, and W. Y. Choi, "Modulation Linearity Characterization of Si Ring Modulators," Journal of Lightwave Technology, 2021, doi: 10.1109/JLT.2021.3093463.

[21] E. Weckenmann et al., "Frequency Chirp Characterization of Silicon Ring Resonator Modulators," IEEE Photonics Technology Letters, vol. 34, no. 12, pp. 653–656, Jun. 2022, doi: 10.1109/LPT.2022.3179650.

[22] Y. Ban *et al*., "Highly Optimized O-band Si Ring Modulators for Low-Power Hybrid CMOS-SiPho Transceivers," *2023 Optical Fiber Communications Conference and Exhibition (OFC)*, San Diego, CA, USA, 2023, pp. 1-3, doi: 10.1364/OFC.2023.W3D.5.

[23] P. M. Seiler et al., "Multiband Silicon Photonic ePIC Coherent Receiver for 64 GBd QPSK," Journal of Lightwave Technology, vol. 40, no. 10, pp. 3331–3337, May 2022, doi: 10.1109/JLT.2022.3158423.

[24] P. M. Seiler et al., "Monolithically Integrated O-Band Coherent ROSA Featuring 2D Grating Couplers for Self-Homodyne Intra Data Center Links," IEEE Photonics J, vol. 15, no. 3, Jun. 2023, doi: 10.1109/JPHOT.2023.3272476.

[25] K. Voigt, L. Zimmermann, G. Winzer, H. Tian, B. Tillack and K. Petermann, "Fully passive Si-photonic 90° hybrid for coherent receiver applications," 2011 37th European Conference and Exhibition on Optical Communication, Geneva, Switzerland, 2011, pp. 1-3.

[26] A. Awny et al., "A Linear Differential Transimpedance Amplifier for 100-Gb/s Integrated Coherent Optical Fiber Receivers," IEEE Trans Microw Theory Tech, vol. 66, no. 2, pp. 973–986, Feb. 2018, doi: 10.1109/TMTT.2017.2752170.

[27] G. Dziallas, A. Fatemi, A. Peczek, L. Zimmermann, A. Malignaggi, and G. Kahmen, "A 56-Gb/s Optical Receiver with 2.08-µA Noise Monolithically Integrated into a 250-nm SiGe BiCMOS Technology," IEEE Trans Microw Theory Tech, vol. 70, no. 1, pp. 392–401, Jan. 2022, doi: 10.1109/TMTT.2021.3104838.

[28] F. P. Guiomar, M. A. Fernandes, J. L. Nascimento, V. Rodrigues, and P. P. Monteiro, "Coherent Free-Space Optical Communications: Opportunities and Challenges," Journal of Lightwave Technology, vol. 40, no. 10, pp. 3173–3186, May 2022, doi: 10.1109/JLT.2022.3164736.

[29] Andrews, Larry C., and Ronald L. Phillips. "Laser beam propagation through random media." *Laser Beam Propagation Through Random Media: Second Edition* (2005), doi: 10.1117/3.626196.

[30] G. Georgieva, P. M. Seiler, C. Mai, A. Peczek, K. Petermann and L. Zimmermann, "A Polarization-Independent Zig-Zag-Tilted Ovals Grating Coupler in a 0.25 µm Photonic BiCMOS Technology," 2022 European Conference on Optical Communication (ECOC), Basel, Switzerland, 2022, pp. 1-4.

[31] D. S. Ly-Gagnon, S. Tsukamoto, K. Katoh, and K. Kikuchi, "Coherent detection of optical quadrature phase-shift keying signals with carrier phase estimation," Journal of Lightwave Technology, vol. 24, no. 1, pp. 12–20, Jan. 2006, doi: 10.1109/JLT.2005.860477.

[32] I. Fatadin, D. Ives, and S. J. Savory, "Blind equalization and carrier phase recovery in a 16-QAM optical coherent system," Journal of Lightwave Technology, vol. 27, no. 15, pp. 3042–3049, Aug. 2009, doi: 10.1109/JLT.2009.2021961.

Youngkwan Jo received B.S. degree in 2017 in electrical and electronic engineering from Yonsei University, Seoul, South Korea, where he is currently working toward the Ph.D. degree. His research interests include design, modeling, and optimization of Si photonic optical devices for high-speed optical interconnect.

Matthieu Oberon received B.S. degree in 2020 in engineering from CentraleSupélec, Gif-Sur-Yvette, France. He is currently working towards a M.S. degree in electrical engineering at Technical University Berlin, Berlin, Germany as part of a dual degree with his home university CentraleSupélec. He additionally works as a student assistant in the Silicon Photonics Group, Technology Department of IHP—Leibniz Institute für innovative Mikroelektronik, Frankfurt, Germany, where his research focuses on coherent optical communication for space applications.

Anna Peczek is in charge of the silicon photonics optoelectronic laboratory at IHP- Leibniz Institute for High Performance Microelectronics. She received a master's degree in Technical Physics with major in optoelectronics and bachelor's degree in Electronics and Telecommunications from Lodz University of Technology in Poland. In 2014 Anna joined IHP in Germany to work on silicon photonics. Anna is specialized in wafer-level characterization and testing and responsible for silicon photonics measurement services. Already for 10 years Anna is involved in evaluation of optoelectronic circuits and development of novel characterization systems.

Yongjin Ji received the B.S. degree in electrical and electronic engineering from Yonsei University, Seoul, South Korea, in 2020. He is currently with High-Speed Circuits and Systems Laboratory, Yonsei University. His research interests include designing and optimizing Si photonic optical devices for various applications.

Minkyu Kim received B.S. and Ph.D. degrees in electrical and electronic engineering from Yonsei University, Seoul, South Korea, in 2015 and 2021, respectively. His doctoral dissertation concerned the monolithic silicon photonic transmitter with ring modulator and its temperature controller. In 2021, He joined IMEC, Leuven, Belgium. In IMEC, he is currently working on high-speed Si photonic modulator design.

Hyun-Kyu Kim (Graduate Student Member, IEEE) received the B.S. degree in 2017 in electrical and electronic engineering from Yonsei University, Seoul, South Korea, where he is currently working toward the Ph.D. degree. His research interests include Si-based electronic/photonic IC design and highspeed optical interconnect.

Min-Hyeong Kim received the B.S. and Ph.D. degrees in electrical and electronic engineering from Yonsei University, Seoul, South Korea, in 2011 and 2018, respectively. He is currently an Analog Design Engineer with Synopsys Group, working on high-speed interface IP design using GAA or FinFET process, especially for mass production of foundry.

Pascal M. Seiler (biography is not available at the time of publication.)

Stefan Lischke received the B.Sc. and M.Sc. degrees in physics with specialization in semiconductor technology from Technical University Brandenburg, Cottbus, in 2005 and 2007, respectively, and the Ph.D. degree in physics from Technical University Berlin, Berlin, Germany, in 2017. He is currently a Researcher with the Silicon Photonics Group, Technology Department of IHP—Leibniz Institute für innovative Mikroelektronik, Frankfurt, Germany. His current work is focused on Germanium photo detectors and the integration of photonic devices into IHP's photonic BiCMOS technology. He was recipient of several best paper awards.

Christian Mai received the master's degree in physics from Technical University Cottbus, Cottbus, Germany, in 2012. He is currently a Researcher with Technology Department, IHP—Leibniz Institute für innovative Mikroelektronik, Frankfurt, Germany. His research is focuses on the monolithic integration of silicon photonics components in the established 0.25-µm BiCMOS technology of the IHP for the development of an electronic photonic integrated circuits technology.

Lars Zimmermann (Senior Member, IEEE) was born in Germany. He received a higher education (undergraduate) from Friedrich-Schiller University, Jena, Germany, Brunel University London, London, U.K., and TU Delft, Delft, The Netherlands, and the Ph.D. degree from IMEC, Leuven, Belgium, in 2003. He moved to Belgium for his postgraduate studies at Katholieke Universiteit Leuven. In Leuven, he was affiliated with IMEC, where he worked for five years. His scientific work at IMEC dealt with the development of extended short-wave infrared detector arrays and sensor assembly processes. In 2004, he moved to TU Berlin. In Berlin, he worked for five years on silicon-based optical motherboard technology, realizing early hybrid assemblies of silicon waveguides with lasers, semiconductor optical amplifiers, and detectors. In 2008, he moved to IHP, the Leibniz Institute für innovative Mikroelektronik. At IHP, he directs the silicon photonics activities. In 2018, he re-joined TU Berlin, where he is currently a Professor in the field of silicon photonics. He is also a Team Leader Silicon photonics at IHP, coordinating the cooperation with TU Berlin in the field of Silicon photonics within the frame of the Joint Lab Silicon Photonics. His current work is focusing on high-performance photonic-electronic integration for optical communications and for nonlinear optical signal processing.

Woo-Young Choi (Member, IEEE) received the B.S., M.S., and Ph.D. degrees in electrical engineering and computer science from the Massachusetts Institute of Technology, Cambridge, MA, USA, in 1986, 1988, and 1994, respectively. His doctoral dissertation concerned the investigation of molecular-beam epitaxy-grown InGaAlAs laser diodes for fiber-optic applications. From 1994 to 1995, he was a Postdoctoral Research Fellow with NTT Opto-Electronics Laboratories, where he worked on femtosecond alloptical switching devices based on low-temperature grown InGaAlAs quantum wells. In 1995, he joined the Department of Electrical and Electronic Engineering, Yonsei University, Seoul, South Korea, where he is currently a Professor. His research interests include high-speed circuits and systems that include high-speed optoelectronics, high-speed electronic circuits, and silicon photonics.